

# Geophysical Research Letters

## RESEARCH LETTER

10.1029/2020GL092370

### Key Points:

- There exists a positive correlation between rainfall over Central Equatorial Africa (CEA) and Indian Ocean Dipole (IOD) during September–December
- Positive IOD events increase rainfall amount and frequency by modifying the Walker circulation, moisture, and the Madden-Julian Oscillation
- Increasing CEA rainfall during the last two decades is potentially attributed to increasing influence of IOD

### Supporting Information:

Supporting Information may be found in the online version of this article.

### Correspondence to:




Y. Jiang,  
[yjiang6@albany.edu](mailto:yjiang6@albany.edu)

### Citation:

Jiang, Y., Zhou, L., Roundy, P. E., Hua, W., & Raghavendra, A. (2021). Increasing influence of Indian Ocean Dipole on precipitation over Central Equatorial Africa. *Geophysical Research Letters*, 48, e2020GL092370. <https://doi.org/10.1029/2020GL092370>

Received 6 JAN 2021  
 Accepted 6 APR 2021

## Increasing Influence of Indian Ocean Dipole on Precipitation Over Central Equatorial Africa

Yan Jiang<sup>1</sup> , Liming Zhou<sup>1</sup> , Paul E. Roundy<sup>1</sup>, Wenjian Hua<sup>2</sup>, and Ajay Raghavendra<sup>1</sup> 

<sup>1</sup>Department of Atmospheric and Environmental Sciences, University at Albany, State University of New York, Albany, NY, USA, <sup>2</sup>Key Laboratory of Meteorological Disaster, Ministry of Education, Nanjing University of Information Science and Technology, Nanjing, China

**Abstract** Using observational rainfall datasets, we identify a positive correlation between precipitation over Central Equatorial Africa (CEA) and the Indian Ocean Dipole (IOD) during September–December (SOND) for the period 1981–2019. Rainfall amount significantly increases during positive IOD events. The enhancement in precipitation is primarily attributed to increased rainfall frequency and reaches the maximum in October. IOD impacts rainfall via modifying the Walker circulation over the tropical Indian Ocean and moisture in the middle troposphere over CEA. The Madden-Julian Oscillation (MJO) activity covaries with IOD to modulate the African Easterly Jet, which is critical to convection development over CEA. SOND rainfall has increased for the last two decades, which is concurrent with increases in both the IOD index and the correlation between IOD and rainfall. The IOD-congruent rainfall changes potentially account for much of rainfall trends in southern and eastern CEA.

**Plain Language Summary** Tropical Africa is one of the convective hotspots. Understanding causes of rainfall variations is crucial for both local ecosystem and rainfall-fed agriculture and society. Here we show that there is a significant positive correlation between CEA rainfall and Indian Ocean Dipole (IOD) during SOND. During positive IOD events, the warmer western Indian Ocean favoring stronger convection and wetter atmosphere to increase rainfall amount and frequency. An increase in rainfall has been observed since the 1990s and is concurrent with the increasing correlation between IOD and rainfall. The increasing IOD index might contribute to much of the rainfall trends over the western, southern, and eastern basin. Thus, IOD variability would provide indications for improving seasonal weather predictions under the changing climate and agricultural developments in CEA.

### 1. Introduction

Central equatorial Africa (CEA) hosts the world's second largest rainforest. Disturbances in interannual or seasonal rainfall not only affect the hydrological cycle, but also have far-reaching impacts on the global carbon cycle (James et al., 2013; Mitchard, 2018). A widespread long-term drought has been observed in the Congo Basin during April–June since the 1980s (Hua et al., 2016; Jiang et al., 2019; Zhou et al., 2014). The drought has been associated with sea surface temperature (SST) anomalies, with declined moisture transport from the Indian Ocean during April–June (Hua et al., 2016). The suppressed ascent over the basin was induced by the westward extended Walker circulation caused by the La Niña-like SST anomalies during 1980–2014 (Hua et al., 2018; Ma & Zhou, 2016). Understanding connections between CEA rainfall and tropical oceans is thus important but challenging due to complex land-atmosphere-ocean interactions, which vary by season and are complicated by teleconnections among oceans (Bush et al., 2020; Otto et al., 2013).

CEA is characterized by a bimodal rainfall pattern with two rainy seasons during March–May and September–November (Jiang et al., 2019). Influences of tropical oceans on CEA rainfall are seasonally specific. The El Niño Southern Oscillation (ENSO) refers to the irregular periodic variations in SSTs over the tropical Pacific Ocean and zonal pressure gradient between tropical western and eastern Pacific Ocean (Wang, 2018). It is negatively correlated with rainfall anomalies in western equatorial Africa during February–August. Positive phase (El Niño) would thus suppress rainfall. The Indian Ocean Dipole (IOD) presents interannual variation in the difference between SST anomalies of tropical western and eastern Indian Ocean featured with changes in zonal winds along the equatorial Indian Ocean (Saji et al., 1999). Positive IOD modes refer to the warmer western Indian Ocean and are associated with reduced rainfall during dry seasons in CEA,

but increased rainfall during September–November and decreased rainfall during March–May in eastern Africa (Nicholson & Dezfuli, 2013; Otto et al., 2013; Shaaban & Roundy, 2017; Todd & Washington, 2004). High tropical Atlantic SSTs could enhance CEA rainfall in dry seasons (Otto et al., 2013). In addition to the teleconnections between tropical SSTs and CEA rainfall, active interactions among different climate models like ENSO and IOD exist and can enhance or suppress their individual effects on rainfall (Nicholson, 2000, 2001; Williams & Hanan, 2011). Simple linear correlation analysis has been commonly used in previous work to quantify the impacts of individual oceanic modes on CEA rainfall (Nicholson & Dezfuli, 2013; Todd & Washington, 2004), while the confounding effects of different modes are often not considered. Hence, previous results might underestimate or overestimate a single mode's independent influence without isolating potential contributions from other modes.

Aside from tropical SSTs, CEA rainfall is also affected by intra-seasonal variabilities. The Madden Julian Oscillation (MJO) is the dominant sub-seasonal mode (20–100 days) in the tropics (Wilson et al., 2013). The MJO becomes the strongest in boreal winter and spring and reaches its second peak in boreal summer (Zhang & Dong, 2004). It affects tropical precipitation year-round and can cause 20%–50% daily precipitation variability within a single season (Berhane et al., 2015). At longer time scales, the MJO has contributed ~14% to the CEA drying trend and interacts with other climate modes by either triggering a large-scale mode like the ENSO or mediating its teleconnections (Hoell et al., 2014; Raghavendra et al., 2020; Zhang, 2005). In reverse, the MJO is modulated by the ENSO and IOD, for it is most active in the Indian and western Pacific oceans (Zaitchik, 2017). Considering interactions between MJO and climate modes is more useful for long-range weather predictions than considering individual modes alone (Roundy et al., 2010). Shimizu et al. (2017) suggested that ENSO's impact on South American rainfall depends on the MJO. Recent studies raised the possibility that MJO might be the mechanism for ENSO to affect Eastern African rainfall (Berhane, 2016; Pohl & Matthews, 2007). Positive IOD events are associated with suppressed MJO convection, while negative IOD events are associated with enhanced MJO convection in the Indian Ocean (Kug et al., 2009; Wilson et al., 2013). Covariance of MJO activity with the IOD could impact its influence on African rainfall. However, few studies have addressed this topic so far (Zaitchik, 2017).

The paucity of high-quality long-term rainfall datasets is another obstacle for previous studies on central Africa rainfall (Washington et al., 2013). Potential secular variations in the relationships between climate models and rainfall in monsoon regions and watershed have been noted (Kumar et al., 1999; Nicholson, 2001; Yadav et al., 2009), but are seldom addressed in CEA due to sparse gauge density. By taking the advantage of a newly created gauge-based precipitation data set (Nicholson et al., 2018), this study applied partial correlation and regression analyses to quantify IOD's impact on rainfall in CEA (10°E–32°E, 8°N–10°S). It presents evidence for a robust positive partial correlation between CEA rainfall and IOD during the September–December (SOND) rainy season. Here we aim to address three questions: (1) how is IOD associated with CEA rainfall amount, frequency, and intensity? (2) what are the physical processes of IOD's impact on rainfall? (3) have the changes in IOD affected the boreal rainfall trend? The results would help to disentangle oceanic impacts on CEA rainfall and to understand rainfall variations, thus improve regional precipitation predictions.

## 2. Data and Methods

### 2.1. Rainfall Datasets

To quantify the correlation between precipitation and climate modes, a newly created gauge-based monthly precipitation product at 2.5° spatial resolution (NIC131, 1921–2014) covering the Congo Basin and surrounding regions was used (Nicholson et al., 2018). The NIC131 was gridded by combining the gauge data at 1,826 individual stations, which is much greater than any existing precipitation datasets over Central Africa, via a statistical reconstruction approach to provide reliable records. To bolster the robustness of the results, another long-term observational monthly rainfall data set from the Global Precipitation Climatology Center (GPCC v2018, 1891–2016) at 1.0° spatial resolution was utilized as well (Schneider et al., 2018).

Given limited temporal and spatial resolutions of both observational datasets, a daily precipitation data set from the Climate Hazards Group Infrared Precipitation with Station Data (CHIRPS2, 1981–present) at 0.25° resolution (Funk et al., 2015) was used. Merged with African gauge data and thermal infrared observations

from geostationary satellites, CHIRPS2 can provide good spatial coverage and temporal records for the study region. It has been validated as the best satellite-derived rainfall product for CEA (Nicholson et al., 2019). CHIRPS2 was used to quantify associations between climate models and rainfall frequency, intensity, and extreme rainfall events.

A rainy day was defined when daily rainfall amount is larger than 1 mm. Rainfall frequency was defined as the percentage of rainy days during study period (Dai et al., 2020; Guan et al., 2018). Rainfall intensity, defined as precipitation rate, was only calculated for rainy days receiving rainfall at least 1 mm per day. Extreme wet and dry rainfall events were identified as those exceeding the 75th and those lower than the 25th percentile of basin-wide daily rainfall during 1981–2019 (Shimizu et al., 2017).

## 2.2. Ocean SST and MJO Indices

Four monthly SST indices from the National Oceanic and Atmospheric Administration were used (Table S1): The Oceanic Niño index (ONI; 1950–present), the Dipole Mode Index (DMI; 1870–present; Saji & Yamagata, 2003a), the Tropical Northern Atlantic Index (TNA; 1948–present) and Tropical Southern Atlantic Index (TSA; 1948–present; Enfield et al., 1999). Positive ONI values indicate El Niño events. Positive DMI values indicate the warmer western Indian Ocean than the east and positive IOD events. Positive values for TNA and SNA indicate high SSTs in corresponding regions. The monthly surface wind data from the Comprehensive Ocean-Atmosphere Data Set (COADS, 1960–present) observation at 1.0° resolution was used as an auxiliary product to estimate oceanic modes (Freeman et al., 2017).

To estimate the status of the MJO, the Real-time Multivariate MJO index (RMM, 1974–present; Wheeler & Hendon, 2004) based on the empirical orthogonal function analysis of zonal wind and outgoing longwave radiation (OLR) from the Center for Australian Weather and Climate Research was used. An active MJO day is identified when RMM amplitude is larger than 1 (Raghavendra et al., 2020). A single MJO event can experience eight phases as the convection starts around the western Indian Ocean and propagates eastward (Zhang 2005). This index is not a perfect or a complete representation of MJO signal but has demonstrated usefulness. The convection during different RMM phases was estimated by the daily OLR (1974–2019) data at 2.5° resolution from NOAA as well (Liebmann & Smith, 1996).

To quantify possible impacts of IOD and MJO on large-scale circulations, vertical motion (omega), horizontal winds, and specific humidity were provided by the 3-hourly Modern-Era Retrospective Analysis for Research and Applications, v.2 (MERRA-2, 1980–present) at 0.625° × 0.5° resolution and 42 vertical levels (Gelaro et al., 2017). With improved and updated data assimilation and observing systems, the MERRA-2 reanalysis represents the currently state-of-the-art reanalysis, and its use of a modern satellite database is expected to improve the data quality over observation-limited regions such as CEA (Hua et al., 2016; Molod et al., 2015). For example, it can better capture the major hydrological characteristics and large-scale circulation patterns over CEA than other reanalysis products (Hua et al., 2019).

## 2.3. Statistical Methods

The independent associations between precipitation and tropical SSTs were quantified using partial correlation analysis. The partial correlation analysis was conducted during four seasons. All variables were detrended before the analysis was applied. Two-sided Pearson test was applied to assess whether correlations were statistically significant. Composite analysis was further applied to analyze rainfall variations and potential modifications in synoptic dynamics. Composites of anomalies in rainfall amount, frequency, intensity, extremes, daily OLR, omega, horizontal winds, and specific humidity were compared for different IOD and RMM phases. Significance of the difference was tested by Monte Carlo simulation and two-tailed Student t test. Ten positive IOD events (1982, 1983, 1994, 1997, 2006, 2008, 2011, 2012, 2018, 2019) and ten negative IOD events (1981, 1989, 1992, 1996, 1998, 2001, 2005, 2010, 2014, 2016) were identified based on the method of Saji and Yamagata (2003b): (1) DMI, zonal wind over Indian Ocean ( $U_{eq}$ , 70°E–90°E, 5°N–5°S), and SST anomaly (SSTA) over the eastern Indian Ocean (90°E–110°E, 0°–10°S) were detrended. (2) A 3-month running mean was applied. (3) DMI,  $U_{eq}$ , and SSTA were all required to exceed 0.5 standard deviation threshold for at least 3 months.

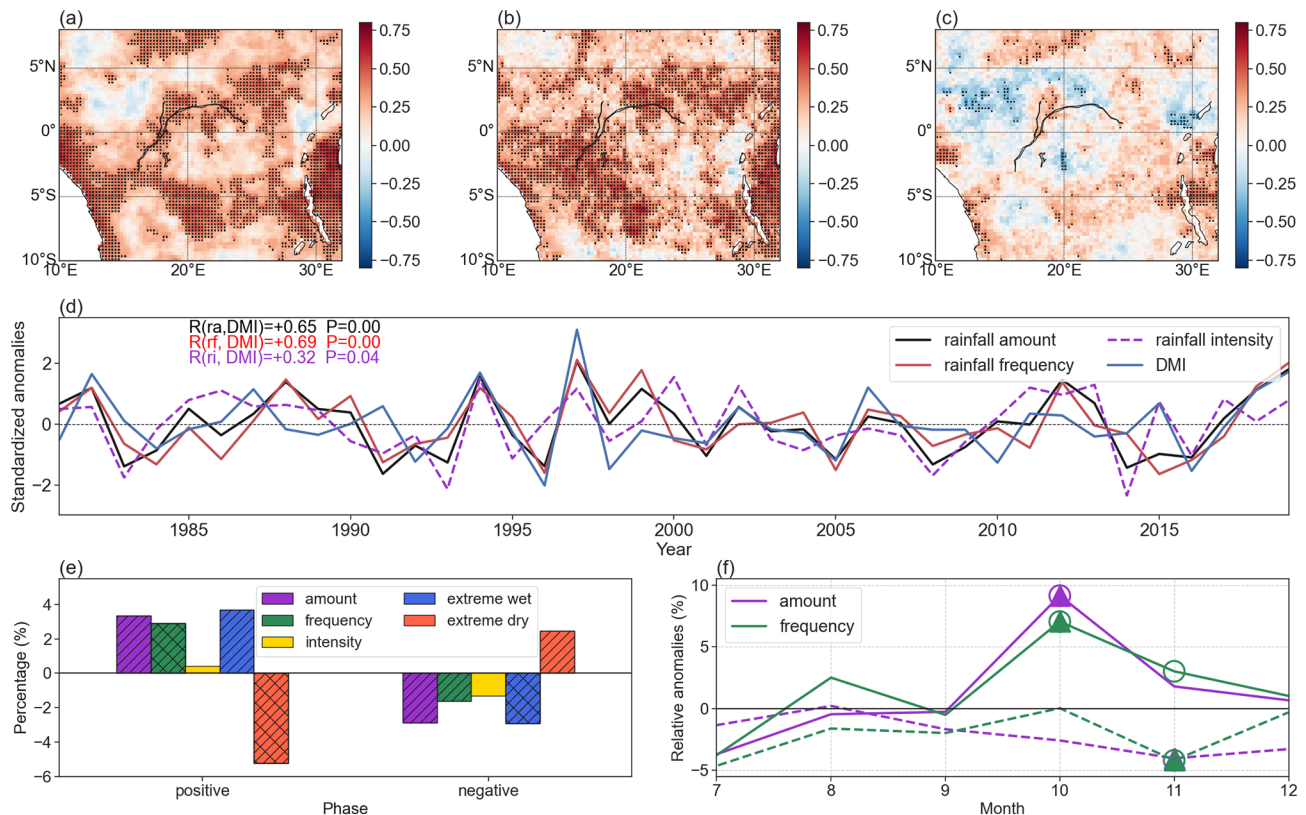


**Figure 1.** Correlations between CEA rainfall and the DMI during September–December for the period 1981–2019. Spatial patterns of partial correlations between the DMI and (a) Rainfall amount, (b) Rainfall frequency, and (c) Rainfall intensity. Grid boxes with dots indicate statistical significance at the 95% confidence level. (d) Interannual variations in the DMI, rainfall amount, frequency, and intensity. The partial correlation coefficients between the DMI and rainfall characteristics and significance levels are shown as well. (e) Relative anomalies of rainfall amount, frequency, intensity, and frequency of extreme rainfall events during positive and negative IOD events. Color bars marked with hatched lines indicate significant at the 95% confidence level tested by Monte Carlo simulation. Color bars with cross lines indicate the significance verified by both Monte Carlo simulation and the two-tailed Student *t* test. (f) Relative anomalies of monthly rainfall amount and frequency during positive IOD (solid lines) and negative events (dashed lines). Points marked by circles indicate significance at the 95% confidence level tested by Monte Carlo simulation. Points marked by triangles indicate significance at the 95% confidence level tested by Student *t* test. CEA, Central Equatorial Africa; DMI, Dipole Mode Index; IOD, Indian Ocean Dipole.

### 3. Results

#### 3.1. Associations of the IOD with CEA Rainfall

In general, the tropical Indian and Pacific Oceans have higher correlations with CEA rainfall than the other oceans, which implies potential stronger impacts on precipitation (Table S2). Negative correlation between precipitation and ONI was observed during June–November, indicating that positive ENSO events are associated with suppressed precipitation. The DMI is positively correlated with precipitation, particularly during September–November when the correlation coefficient reaches 0.68 ( $P < 0.01$ ). Positive IOD events are thus associated with enhanced precipitation. Correlations between CEA rainfall and tropical Atlantic SSTs are relatively weak. The TNA is negatively correlated with precipitation during March–May. The tropical southern Atlantic SST is not directly correlated with CEA rainfall. Given the strongest correlation between precipitation and DMI during September–November, the study mainly focused on analyzing IOD’s potential impacts on CEA rainfall during SON. December was also included, for there is a significant correlation in winter and IOD events can last to December (Saji et al., 1999).

Figure 1 displays associations between the DMI and rainfall amount, frequency, and intensity. The DMI is positively correlated basin-wide rainfall amount except the northwestern basin (Figure 1a). Similar spatial patterns are observed by the NIC131 and GPCC data (Figure S1). Discrepancies over the central and southern basin might be attributed to the differences in data sources, resolutions, and interpolation methods of

these three rainfall products. The positive correlation is seen between the DMI and rainfall frequency as well (Figure 1b). DMI is positively correlated with rainfall intensity in the southern and eastern basin but is negatively correlated with intensity in the northwest (Figure 1c), resulting in an overall weak association with rainfall intensity. Consistent with the spatial patterns, regionally averaged rainfall amount is positively correlated with DMI ( $R = 0.69$ ,  $P < 0.01$ ). The coefficient between rainfall frequency and DMI reaches 0.65 ( $P < 0.01$ ) (Figure 1d).

Next, composites of anomalies in rainfall amount, frequency, intensity, and the frequency of extreme events were calculated for positive and negative IOD events (Figure 1e). Regional mean precipitation amount is significantly enhanced by  $\sim 3.4\%$  during positive IOD events but is suppressed by  $\sim 3\%$  during negative IOD events. Rainfall frequency is increased by  $\sim 3\%$  during positive IOD events but is decreased by  $\sim 2\%$  during negative IOD events. Given that the relative change in rainfall amount ( $A$ ) can be attributed to the relative changes in rainfall frequency ( $F$ ) and intensity ( $I$ ) ( $dA/A = dF/F + dI/I$ ), the increased rainfall amount is thus mainly attributed to the increased rainfall frequency during positive IOD events. Although there is less change in rainfall intensity during active IOD events, the frequency of extreme wet rainfall events is evidently increased by 4% and the frequency of extreme dry events is decreased by 5% during positive IOD events.

Seasonal phase locking is an important characteristic of IOD. An IOD event intensifies after June, peaks in October, and rapidly decays during November–December (Saji et al., 1999). Impacts of IOD on rainfall was further estimated during different months. Figure 1f shows that the changes in rainfall amount and frequency induced by IOD are highest during October and November. Rainfall amount and frequency increase by  $\sim 9\%$  and  $\sim 7\%$  during positive IOD events in October, which is consistent with IOD's evolution.

### 3.2. Impacts of IOD on MJO Activity and Mean Circulations

To investigate possible physical processes of IOD's impacts on CEA rainfall, covaried MJO activity and modifications in mean circulations were estimated. The MJO is most active during SON, when active MJO days dominate about two thirds of the time (Table S3). First, we composited rainfall based on days with active MJOs and days without active MJO during positive and negative IOD events respectively (Figure 2a). It is shown that rainfall amount increases by  $\sim 4\%$  with active MJO, while only increases by  $\sim 2\%$  without active MJO during positive IOD events. Consistently, rainfall frequency and the frequency of extreme wet events increase by  $\sim 3.5\%$  and  $\sim 4.5\%$  during active MJO days. MJO activity is likely a crucial process through which IOD impacts CEA rainfall. During negative IOD events, MJO activity slightly alleviates the IOD's suppression effect on precipitation, as the decrease in rainfall amount reaches  $\sim 3.5\%$  without MJO impacts. Spatial maps of rainfall variations, which were calculated as the differences in composite rainfall with or without active MJO between positive and negative IOD events, illustrate that MJO could significantly increase rainfall amount over central and southern CEA (Figures 2b–2d). In general, the net effect of MJO tends to enhance precipitation over CEA, and the impact is stronger during positive IOD events.

Next, the difference in composite vertical motion, horizontal wind, and specific humidity between positive and negative IOD events were assessed. CEA rainfall is influenced by the Walker circulation (Hua et al., 2016, 2018) with its upward branch located over CEA and two downward branches over the western Indian Ocean around  $40^{\circ}\text{E}$ – $55^{\circ}\text{E}$  and the Gulf of Guinea. Moisture converges in the lower troposphere, and the low-level easterly jet (800–600 hPa) favors convection developments over CEA (Figure S2). During positive IOD events, the Walker circulation becomes weaker (Figures 2e and S3). More moisture is transported and accumulated at lower and middle troposphere over CEA via abnormal easterlies (Figures 2e, 2g, S4e and S5e). During negative IOD events, the Walker circulation is strengthened and westward extended (Figure S3). The mid-level troposphere becomes drier over CEA (Figure S4). Figure 2f shows the differences in composite variables with active MJO. The moistening in lower and middle troposphere during positive IOD events is more constrained over eastern Africa and the western Indian Ocean. And the easterly jet is weakened particularly during negative IOD events and thus is less favorable for convection systems (Figures 2f and S5d).

In view of MJO's impacts on synoptic dynamics during IOD events, IOD modifications on MJO activity were analyzed. Active MJO days were clarified as wet or dry phases if CEA rainfall was significantly

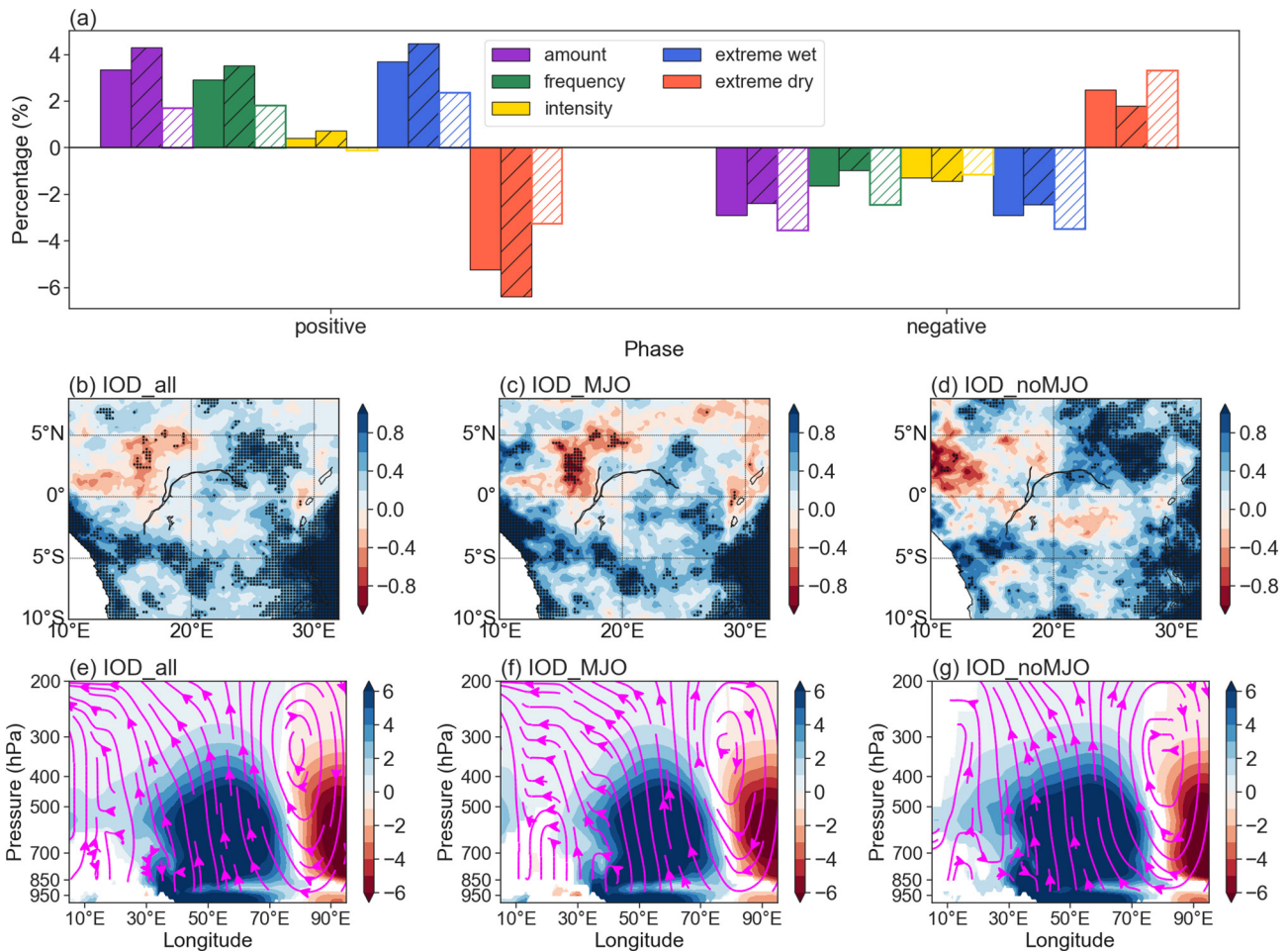


**Figure 2.** Modified impacts of IOD on CEA rainfall by MJO during SOND. (a) Relative anomalies of rainfall amount, frequency, intensity, and frequency of extreme rainfall events during positive and negative IOD events. Solid color bars with hatched lines present rainfall anomalies with MJO influences. Color bars with only hatched lines present rainfall anomalies without MJO impacts. Spatial patterns of differences in rainfall amount between (b) Positive and negative IOD events, (c) Positive and negative IOD events with active MJO, (d) same as (c) but without MJO activities. Grid boxes with dots indicate statistical significance at the 95% confidence level. Composites of differences in vertical cross section (10°N–10°S) of specific humidity ( $10^{-1} \text{ g}\cdot\text{kg}^{-1}$ , shaded), streamlines of zonal wind ( $u$ , m/s) and omega ( $10^{-1} \text{ Pa}\cdot\text{s}^{-1}$ ) between (e) Positive and negative IOD events, (f) positive and negative IOD events with active MJO, (g) Same as (f) but without active MJO. Only significant differences at 95% confidence level are plotted. CEA, Central Equatorial Africa; DMI, Dipole Mode Index; IOD, Indian Ocean Dipole; MJO, Madden-Julian Oscillation.

enhanced or suppressed. In this way, phases 1 and 2 (MJO convection over the western Indian Ocean) are wet phases, while phases 4, 5, and 6 (MJO convection over the eastern Indian Ocean and Maritime Continent) are dry phases. Compared with neutral IOD events, there are more wet phases days during positive IOD events, and slightly more dry phases days during negative IOD events (Table S3). Composite synoptic dynamics anomalies for wet MJO phase during positive IOD events indicate that low- and mid-level easterly anomalies are stronger, the lower atmosphere is moister over the western and central Indian Ocean and the Walker circulation is much weakened during positive IOD events, resulting in stronger convection over CEA (Figures S6e–S6h). During negative IOD events, increased convection is constrained over eastern Africa attributed to MJO (Figures S6i–S6l). For dry phases, the stronger subsidence limb of the Walker circulation occurs eastward over the central Indian Ocean and the abnormal low and mid-level westerlies become stronger over both CEA and tropical Indian Ocean during negative IOD events. As a result, slightly increased moisture is observed above CEA and MJO's suppression effect on convection over CEA is weakened (Figure S7).

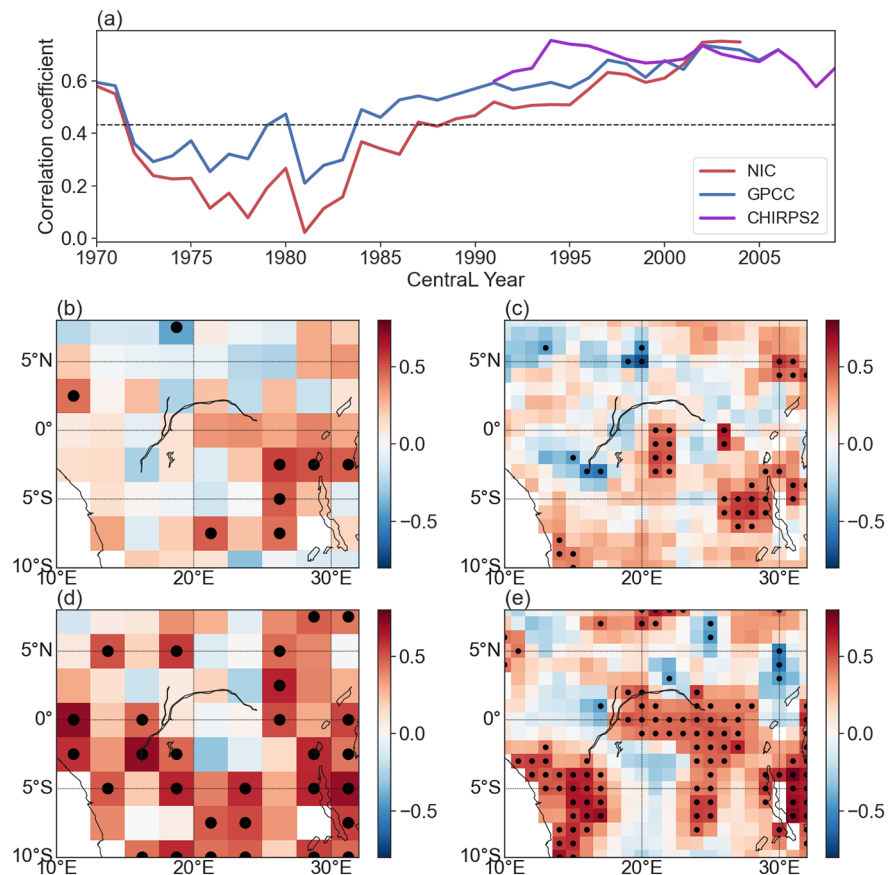


**Figure 3.** (a) 21-year sliding partial correlations between the DMI and SOND rainfall amount for the period 1960–2019. The black dashed line indicates significance at 95% confidence level. Spatial patterns of partial correlations between the DMI and rainfall estimated by (b) NIC131 and (c) GPCC during 1967–1990 (d)–(e) Same as (b)–(c) but during 1991–2014. Grid boxes with dots indicate correlations are significant at the 95% confidence level. DMI, Dipole Mode Index.

### 3.3. Impacts of Changing IOD on CEA Rainfall Trend

A warmer tropical Indian ocean was projected by climate models and observations showed faster SST warming in the western Indian Ocean than in the east since the 1960s (Cai et al., 2013; Vecchi & Soden, 2007). Accompanying this warming trend, an increasing DMI has been documented. The frequency and intensity of positive IOD events have increased during the 20th century (Abram et al., 2008; Cai et al., 2009, 2014). This raises a question regarding whether IOD impacts on CEA rainfall would also change?

To quantify potential secular variation in the association between IOD and CEA rainfall, partial correlation analysis between DMI and rainfall was extended back to the 1960s using long-term observational rainfall data. Sliding correlations on a 21-year moving window between DMI and rainfall were calculated using all three rainfall datasets. The correlation coefficient has increased since the 1970s, and it has steadily reached above 0.6 since the late 1980s (Figure 3a). Spatial patterns of partial correlation show that the correlations were much weaker during 1967–1990. Significant positive correlations were only observed over the south-eastern basin (Figures 3b and 3c). While for the recent two decades, stronger positive correlations were discovered with extended coverage including the western and southern basin (Figures 3d and 3e). Changes in spatial correlation maps suggest stronger potential impacts of IOD on rainfall.

Considering the stronger correlation between the DMI and precipitation, possible changes in rainfall and contributions from the IOD were assessed. Figure 4a shows that there are more grids showing increasing rainfall trends since 1991 compared to the earlier period 1967–1990. Next, rainfall trends were estimated at both basin and grid levels. Regional averaged rainfall has increased by 0.01–0.02 mm·d<sup>-1</sup>·yr<sup>-1</sup> ( $P < 0.05$ )

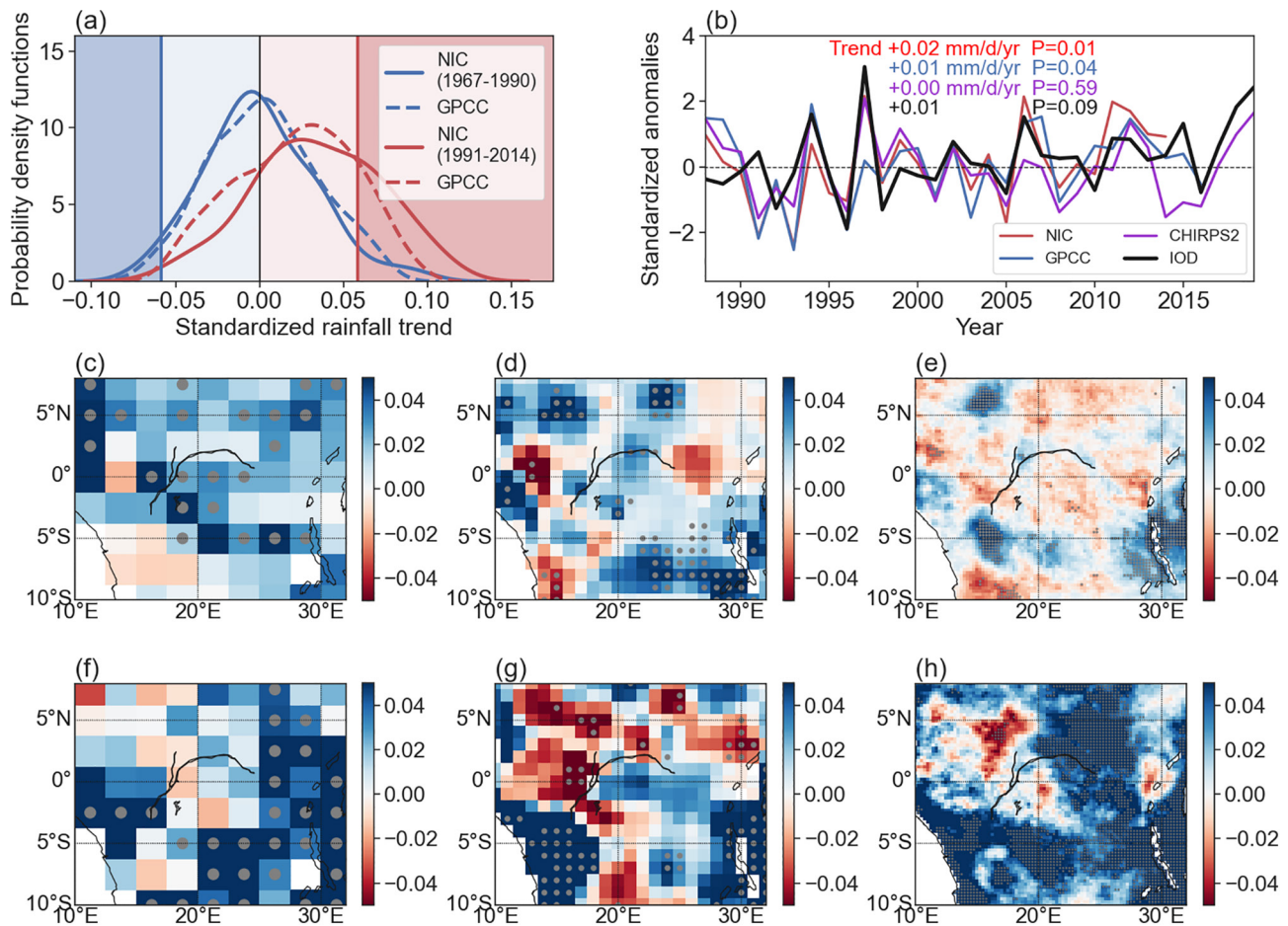


**Figure 4.** (a) Probability density functions of standardized SOND rainfall trends estimated by NIC131 (solid lines) and GPCC (dashed lines) within CEA during 1967–1990 (blue lines) and 1991–2014 (red lines). Dark red and blue shades indicate grids with significant trends at the 95% confidence level. (b) Interannual variations and linear trends of the DMI and rainfall during SOND since 1991. Linear trends and significance levels are shown. Spatial pattern of linear trends in SOND rainfall ( $\text{mm}\cdot\text{d}^{-1}\cdot\text{yr}^{-1}$ ) estimated by (c) NIC131, (d) GPCC, and (e) CHIRPS2 during 1991–2014. Grid boxes with dots have a significant trend at 95% confidence level. Interannual rainfall changes ( $\text{mm}\cdot\text{d}^{-1}\cdot\text{yr}^{-1}$ ) congruent with the DMI trend estimated by (f) NIC131, (g) GPCC, and (h) CHIRPS2 during 1991–2014. Grid boxes with dots indicate the regression are significant at 95% confidence level. DMI, Dipole Mode Index.

since 1991 featured with an increasing DMI (Figure 4b). Spatial patterns of rainfall trends show that the wetting is strong over northern, central, and southeastern CEA, though CHIRPS2 data observed weaker increasing trends. The maximum increasing rate reaches above  $0.04\text{ mm}\cdot\text{d}^{-1}\cdot\text{yr}^{-1}$  (Figures 4c–4e). To quantify the sensitivity of rainfall to IOD, we adopted the method following Cai et al. (2009): First, detrended rainfall anomalies were regressed onto the detrended DMI to quantify IOD impacts on rainfall. Then, the regression coefficients were multiplied with the DMI trend to yield rainfall changes congruent with the increasing DMI. The results suggest that impact of IOD is strong over western, southern, and eastern CEA, which are consistent with previous partial correlation results. The IOD trend-congruent rainfall increase is comparable with the observed rainfall increases in the western, southern, and eastern basin, while the IOD-congruent rainfall decrease over the northwestern CEA was observed by GPCC and CHIRPS2 data (Figures 4f–4h).

#### 4. Discussions and Conclusions

Using observational rainfall datasets, we have shown a robust positive correlation between SOND precipitation over CEA and IOD during 1981–2019, which was little addressed in previous studies. The correlation coefficient between DMI and regional averaged rainfall reaches 0.65 ( $P < 0.01$ ). Rainfall amount, frequency, and the frequency of extreme rainfall events significantly increased during positive IOD events and decreased during negative IOD events. Consistent with the seasonal phase locking of IOD, the enhancement



in rainfall amount and frequency peaks during October and the suppression of precipitation is stronger during November. In general, the enhancement associated with positive IOD events is stronger than the suppression associated negative IOD events, which might be attributed to the generally greater amplitude of positive IOD events (Cai et al., 2013).

Changes in rainfall activity associated with the IOD are likely via modifications of mean circulations, moisture distribution, and MJO activity. Composite analysis indicates that increased rainfall during positive IOD events is featured with a weaker Walker circulation, which is consistent with previous studies manifesting contributions of a strengthened Walker circulation to drought in CEA (Hua et al., 2016, 2018). Following the change in the Walker circulation, moisture increases in the lower and middle troposphere over CEA. MJO activity covaries with the IOD to influence CEA rainfall as well, which was less addressed when quantifying oceanic influences on rainfall or interactions between the MJO and the IOD. There are likely more wet MJO days during positive IOD events and more dry MJO days during negative IOD events, which are consistent with previous studies indicating higher SST favoring the development of certain MJO convection (Kug et al., 2009; Wilson et al., 2013). Anomalies in the Walker circulation and moisture distribution are amplified by MJO activity. Enhancement of convection over CEA is stronger within wet MJO days during positive IOD events. During negative IOD events, the easterly jet over CEA is weakened, while slightly more moisture is transported to the basin during dry MJO days. As a result, the net MJO impacts are more likely to increase precipitation during active IOD events, particularly for positive IOD events. Interannual variability of the IOD would thus provide useful indications to understand rainfall variability and conduct reliable rainfall prediction in the changing climate over CEA.

Given the important role of IOD-MJO interactions on precipitation, further research on interactions between sub-seasonal variability and interannual variability is required to explicitly understand regional rainfall variability and improve seasonal predictions. Our study found that MJO convection over eastern African and the western Indian ocean (wet phases) are strengthened during positive IOD events, and MJO convection over the eastern Indian Ocean and Maritime Continent (dry phases) are strengthened and eastward shifted during negative years. However, impacts of MJO on CEA rainfall do not simply depends on MJO frequency and convection cores, but also on how the MJO system affects local weather conditions including wind shears and moisture. In addition, there are interactions among IOD and other climatic modes via the atmospheric bridge (Alexander et al., 2002). IOD is positively correlated with ENSO ( $R = 0.75$ ,  $P < 0.01$ ) during September–December. Though an El Niño event is associated with decreased CEA rainfall, it could be concurrent with a positive IOD event which could enhance local rainfall. On the other hand, ENSO affects MJO activity as well. Time lagged correlation analysis indicated that MJO is particularly strong in the Pacific Ocean when an El Niño event develops but is weak in the wake of the El Niño (Zhang & Gottschalk, 2002). MJO convection also tends to shift eastward during El Niño events, and vice versa (Bergman et al., 2001; Hendon et al., 1999). However, specific studies including ENSO-MJO interactions tested few associations with African rainfall. Hence, process-based climate model simulations are further needed to obtain a more nuanced understanding of IOD and ENSO's interactions with sub-seasonal variability and their combined influences on CEA precipitation.

Consistent with previous climate projections, the DMI has increased since the 1960s. Along with the warming Indian Ocean, the positive correlation between DMI and SOND rainfall becomes stronger with time, and an increasing trend in SOND rainfall has been observed since the 1990s as well. The IOD trend-induced rainfall increase are suggested to account for much of the rainfall trend by regression analysis. Aside from increases in DMI and the correlation between IOD and CEA rainfall, the frequency of strong positive IOD events is projected to increase (Cai et al., 2014, 2020). The Walker circulation is predicted to decrease and MJO activity will be modified under the warming climate (Maloney et al., 2019; Vecchi & Soden, 2007). It is possible that variations in CEA rainfall and the correlation between IOD and CEA rainfall are linked with the global warming trend. Although we did not answer how much change in rainfall can be explained by internal variability or anthropogenic warming, our results highlight the necessity and importance of considering the increasing influences of IOD-CEA rainfall relationships into future climate projection and seasonal forecasts of CEA rainfall.

## Data Availability Statement

The CHIRPS2 rainfall data are available at [https://data.chc.ucsb.edu/products/CHIRPS-2.0/global\\_daily/](https://data.chc.ucsb.edu/products/CHIRPS-2.0/global_daily/). The DMI is available at [https://psl.noaa.gov/gcos\\_wgsp/Timeseries/DMI/](https://psl.noaa.gov/gcos_wgsp/Timeseries/DMI/). The ONI can be obtained at <https://www.psl.noaa.gov/data/correlation/oni.data>. TNA data can be downloaded at <https://www.psl.noaa.gov/data/correlation/tna.data> and TSA is available at <https://www.psl.noaa.gov/data/correlation/tsa.data>. The COADS wind data can be downloaded at <https://psl.noaa.gov/data/gridded/data.coads.1deg.html>. The MJO index can be obtained at <http://www.bom.gov.au/climate/mjo/>. MERRA-2 reanalysis data can be obtained from the Goddard Earth Sciences Data and Information Services Center ([https://disc.gsfc.nasa.gov/datasets/M2I3NPASM\\_5.12.4/summary](https://disc.gsfc.nasa.gov/datasets/M2I3NPASM_5.12.4/summary)).

## Acknowledgments

This study was supported by the National Science Foundation (NSF AGS-1535426 and AGS-1854486). The authors acknowledge Dr. Sharen E. Nicholson for providing the NIC131 rainfall data.

## References

- Abram, N. J., Gagan, M. K., Cole, J. E., Hantoro, W. S., & Mudelsee, M. (2008). Recent intensification of tropical climate variability in the Indian Ocean. *Nature Geoscience*, *1*(12), 849–853. <https://doi.org/10.1038/ngeo357>
- Alexander, M. A., Bladé, I., Newman, M., Lanzante, J. R., Lau, N.-C., & Scott, J. D. (2002). The atmospheric bridge: The influence of ENSO teleconnections on air-sea interaction over the global oceans. *Journal of Climate*, *15*(16), 2205–2231. [https://doi.org/10.1175/1520-0442\(2002\)015<2205:tabtio>2.0.co;2](https://doi.org/10.1175/1520-0442(2002)015<2205:tabtio>2.0.co;2)
- Bergman, J. W., Hendon, H. H., & Weickmann, K. M. (2001). Intraseasonal air-sea interactions at the onset of El Niño. *Journal of Climate*, *14*(8), 1702–1719. [https://doi.org/10.1175/1520-0442\(2001\)014<1702:iasiat>2.0.co;2](https://doi.org/10.1175/1520-0442(2001)014<1702:iasiat>2.0.co;2)
- Berhane, F., Zaitchik, B., & Badr, H. S. (2015). The Madden-Julian oscillation's influence on spring rainy season precipitation over equatorial West Africa. *Journal of Climate*, *28*(22), 8653–8672. <https://doi.org/10.1175/jcli-d-14-00510.1>
- Berhane, F. G. (2016). Intraseasonal precipitation variability over tropical Africa (Doctoral dissertation). Johns Hopkins University.
- Bush, E. R., Jeffery, K., Bunnefeld, N., Tutin, C., Musgrave, R., Moussavou, G., et al. (2020). Rare ground data confirm significant warming and drying in western equatorial Africa. *PeerJ*, *8*, e8732. <https://doi.org/10.7717/peerj.8732>
- Cai, W., Cowan, T., & Sullivan, A. (2009). Recent unprecedented skewness toward positive Indian ocean dipole occurrences and its impact on Australian rainfall. *Geophysical Research Letters*, *36*(11). <https://doi.org/10.1029/2009gl037604>
- Cai, W., Santoso, A., Wang, G., Weller, E., Wu, L., Ashok, K., et al. (2014). Increased frequency of extreme Indian ocean dipole events due to greenhouse warming. *Nature*, *510*(7504), 254–258. <https://doi.org/10.1038/nature13327>
- Cai, W., Yang, K., Wu, L., Huang, G., Santoso, A., Ng, B., et al. (2020). Opposite response of strong and moderate positive Indian ocean dipole to global warming. *Nature Climate Change*, *11*(1), 27–32. <https://doi.org/10.1038/s41558-020-00943-1>
- Cai, W., Zheng, X.-T., Weller, E., Collins, M., Cowan, T., Lengaigne, M., et al. (2013). Projected response of the Indian ocean dipole to greenhouse warming. *Nature Geoscience*, *6*(12), 999–1007. <https://doi.org/10.1038/ngeo2009>
- Dai, A., Rasmussen, R. M., Liu, C., Ikeda, K., & Prein, A. F. (2020). A new mechanism for warm-season precipitation response to global warming based on convection-permitting simulations. *Climate Dynamics*, *55*(1), 343–368. <https://doi.org/10.1007/s00382-017-3787-6>
- Enfield, D. B., Mestas-Núñez, A. M., Mayer, D. A., & Cid-Serrano, L. (1999). How ubiquitous is the dipole relationship in tropical Atlantic sea surface temperatures?. *Journal of Geophysical Research*, *104*(C4), 7841–7848. <https://doi.org/10.1029/1998jc900109>
- Freeman, E., Woodruff, S. D., Worley, S. J., Lubker, S. J., Kent, E. C., Angel, W. E., et al. (2017). ICOADS Release 3.0: A major update to the historical marine climate record. *International Journal of Climatology*, *37*(5), 2211–2232. <https://doi.org/10.1002/joc.4775>
- Funk, C., Peterson, P., Landsfeld, M., Pedreros, D., Verdin, J., Shukla, S., et al. (2015). The climate hazards infrared precipitation with stations—A new environmental record for monitoring extremes. *Scientific Data*, *2*(1), 1–21. <https://doi.org/10.1038/sdata.2015.66>
- Gelaro, R., McCarty, W., Suárez, M. J., Todling, R., Molod, A., Takacs, L., et al. (2017). The modern-era retrospective analysis for research and applications, version 2 (MERRA-2). *Journal of Climate*, *30*(14), 5419–5454. <https://doi.org/10.1175/jcli-d-16-0758.1>
- Guan, K., Good, S. P., Caylor, K. K., Medvigy, D., Pan, M., Wood, E. F., et al. (2018). Simulated sensitivity of African terrestrial ecosystem photosynthesis to rainfall frequency, intensity, and rainy season length. *Environmental Research Letters*, *13*(2), 025013. <https://doi.org/10.1088/1748-9326/aa9f30>
- Hendon, H. H., Zhang, C., & Glick, J. D. (1999). Interannual variation of the Madden-Julian oscillation during austral summer. *Journal of Climate*, *12*(8), 2538–2550. [https://doi.org/10.1175/1520-0442\(1999\)012<2538:ivotmj>2.0.co;2](https://doi.org/10.1175/1520-0442(1999)012<2538:ivotmj>2.0.co;2)
- Hoell, A., Barlow, M., Wheeler, M. C., & Funk, C. (2014). Disruptions of El Niño-southern oscillation teleconnections by the Madden-Julian oscillation. *Geophysical Research Letters*, *41*(3), 998–1004. <https://doi.org/10.1002/2013gl058648>
- Hua, W., Zhou, L., Chen, H., Nicholson, S. E., Jiang, Y., & Raghavendra, A. (2018). Understanding the central equatorial African long-term drought using AMIP-type simulations. *Climate Dynamics*, *50*(3–4), 1115–1128. <https://doi.org/10.1007/s00382-017-3665-2>
- Hua, W., Zhou, L., Chen, H., Nicholson, S. E., Raghavendra, A., & Jiang, Y. (2016). Possible causes of the central equatorial African long-term drought. *Environmental Research Letters*, *11*(12), 124002. <https://doi.org/10.1088/1748-9326/11/12/124002>
- Hua, W., Zhou, L., Nicholson, S. E., Chen, H., & Qin, M. (2019). Assessing reanalysis data for understanding rainfall climatology and variability over central equatorial Africa. *Climate Dynamics*, *53*(1–2), 651–669. <https://doi.org/10.1007/s00382-018-04604-0>
- James, R., Washington, R., & Rowell, D. P. (2013). Implications of global warming for the climate of African rainforests. *Philosophical Transactions of the Royal Society B: Biological Sciences*, *368*(1625), 20120298. <https://doi.org/10.1098/rstb.2012.0298>
- Jiang, Y., Zhou, L., Tucker, C. J., Raghavendra, A., Hua, W., Liu, Y. Y., & Joiner, J. (2019). Widespread increase of boreal summer dry season length over the Congo rainforest. *Nature Climate Change*, *9*(8), 617–622. <https://doi.org/10.1038/s41558-019-0512-y>
- Kug, J.-S., Sooraj, K. P., Jin, F.-F., Luo, J.-J., & Kwon, M. (2009). Impact of Indian ocean dipole on high-frequency atmospheric variability over the Indian Ocean. *Atmospheric Research*, *94*(1), 134–139. <https://doi.org/10.1016/j.atmosres.2008.10.022>
- Kumar, K. K., Rajagopalan, B., & Cane, M. A. (1999). On the weakening relationship between the Indian monsoon and ENSO. *Science*, *284*(5423), 2156–2159. <https://doi.org/10.1126/science.284.5423.2156>
- Liebmann, B., & Smith, C. A. (1996). Description of a complete (interpolated) outgoing longwave radiation dataset. *Bulletin of the American Meteorological Society*, *77*(6), 1275–1277.
- Ma, S., & Zhou, T. (2016). Robust strengthening and westward shift of the tropical Pacific Walker circulation during 1979–2012: A comparison of 7 sets of reanalysis data and 26 CMIP5 Models. *Journal of Climate*, *29*(9), 3097–3118. <https://doi.org/10.1175/jcli-d-15-0398.1>

- Maloney, E. D., Adames, Á. F., & Bui, H. X. (2019). Madden-Julian oscillation changes under anthropogenic warming. *Nature Climate Change*, 9(1), 26–33. <https://doi.org/10.1038/s41558-018-0331-6>
- Mitchard, E. T. A. (2018). The tropical forest carbon cycle and climate change. *Nature*, 559(7715), 527–534. <https://doi.org/10.1038/s41586-018-0300-2>
- Molod, A., Takacs, L., Suarez, M., & Bacmeister, J. (2015). Development of the GEOS-5 atmospheric general circulation model: Evolution from MERRA to MERRA2. *Geoscientific Model Development*, 8(5), 1339–1356. <https://doi.org/10.5194/gmd-8-1339-2015>
- Nicholson, S. (2001). Climatic and environmental change in Africa during the last two centuries. *Climate Research*, 17(2), 123–144. <https://doi.org/10.3354/cr017123>
- Nicholson, S. E. (2000). The nature of rainfall variability over Africa on time scales of decades to Millennia. *Global and Planetary Change*, 26(1–3), 137–158. [https://doi.org/10.1016/s0921-8181\(00\)00040-0](https://doi.org/10.1016/s0921-8181(00)00040-0)
- Nicholson, S. E., & Dezfuli, A. K. (2013). The relationship of rainfall variability in western equatorial Africa to the tropical oceans and atmospheric circulation. Part I: The boreal spring. *Journal of Climate*, 26(1), 45–65. <https://doi.org/10.1175/jcli-d-11-00653.1>
- Nicholson, S. E., Klotter, D., Dezfuli, A. K., & Zhou, L. (2018). New rainfall datasets for the Congo basin and surrounding regions. *Journal of Hydrometeorology*, 19(8), 1379–1396. <https://doi.org/10.1175/jhm-d-18-0015.1>
- Nicholson, S. E., Klotter, D., Zhou, L., & Hua, W. (2019). Validation of satellite precipitation estimates over the Congo basin. *Journal of Hydrometeorology*, 20(4), 631–656. <https://doi.org/10.1175/jhm-d-18-0118.1>
- Otto, F. E. L., Jones, R. G., Halladay, K., & Allen, M. R. (2013). Attribution of changes in precipitation patterns in African rainforests. *Philosophical Transactions of the Royal Society B*, 368(1625), 20120299. <https://doi.org/10.1098/rstb.2012.0299>
- Pohl, B., & Matthews, A. J. (2007). Observed changes in the lifetime and amplitude of the Madden-Julian oscillation associated with inter-annual ENSO sea surface temperature anomalies. *Journal of Climate*, 20(11), 2659–2674. <https://doi.org/10.1175/jcli4230.1>
- Raghavendra, A., Zhou, L., Roundy, P. E., Jiang, Y., Milrad, S. M., Hua, W., & Xia, G. (2020). The MJO's impact on rainfall trends over the Congo rainforest. *Climate Dynamics*, 1–13. <https://doi.org/10.1007/s00382-020-05133-5>
- Roundy, P. E., MacRitchie, K., Asuma, J., & Melino, T. (2010). Modulation of the global atmospheric circulation by combined activity in the Madden-Julian oscillation and the El Niño-Southern oscillation during boreal winter. *Journal of Climate*, 23(15), 4045–4059. <https://doi.org/10.1175/2010jcli3446.1>
- Saji, N. H., Goswami, B. N., Vinayachandran, P. N., & Yamagata, T. (1999). A dipole mode in the tropical Indian Ocean. *Nature*, 401(6751), 360–363. <https://doi.org/10.1038/43854>
- Saji, N. H., & Yamagata, T. (2003a). Possible impacts of Indian ocean dipole mode events on global climate. *Climate Research*, 25(2), 151–169. <https://doi.org/10.3354/cr025151>
- Saji, N. H., & Yamagata, T. (2003b). Structure of SST and surface wind variability during Indian ocean dipole mode events: COADS observations. *Journal of Climate*, 16(16), 2735–2751. [https://doi.org/10.1175/1520-0442\(2003\)016<2735:sosasw>2.0.co;2](https://doi.org/10.1175/1520-0442(2003)016<2735:sosasw>2.0.co;2)
- Schneider, U., Becker, A., Finger, P., Meyer-Christoffer, A., Ziese, M. (2018). *GPCC full data monthly product version 2018 at 1.0°: Monthly land-surface precipitation from rain-gauges built on GTS-based and historical data*. Global Precipitation Climatology Centre. [https://doi.org/10.5676/DWD\\_GPCC/FD\\_M\\_V2018\\_100](https://doi.org/10.5676/DWD_GPCC/FD_M_V2018_100)
- Shaaban, A. A., & Roundy, P. E. (2017). OLR perspective on the Indian ocean dipole with application to East African precipitation. *Quarterly Journal of the Royal Meteorological Society*, 143(705), 1828–1843. <https://doi.org/10.1002/qj.3045>
- Shimizu, M. H., Ambrizzi, T., & Liebmann, B. (2017). Extreme precipitation events and their relationship with ENSO and MJO phases over northern South America. *International Journal of Climatology*, 37(6), 2977–2989. <https://doi.org/10.1002/joc.4893>
- Todd, M. C., & Washington, R. (2004). Climate variability in central equatorial Africa: Influence from the Atlantic sector. *Geophysical Research Letters*, 31(23). <https://doi.org/10.1029/2004GL020975>
- Vecchi, G. A., & Soden, B. J. (2007). Global warming and the weakening of the tropical circulation. *Journal of Climate*, 20(17), 4316–4340. <https://doi.org/10.1175/jcli4258.1>
- Wang, C. (2018). A review of ENSO theories. *National Science Review*, 5(6), 813–825. <https://doi.org/10.1093/nsr/nwy104>
- Washington, R., James, R., Pearce, H., Pokam, W. M., & Moufouma-Okia, W. (2013). Congo Basin rainfall climatology: Can we believe the climate models?. *Philosophical Transactions of the Royal Society B: Biological Sciences*, 368(1625), 20120296. <https://doi.org/10.1098/rstb.2012.0296>
- Wheeler, M. C., & Hendon, H. H. (2004). An all-season real-time multivariate MJO index: Development of an index for monitoring and prediction. *Monthly Weather Review*, 132(8), 1917–1932. [https://doi.org/10.1175/1520-0493\(2004\)132<1917:aarmmi>2.0.co;2](https://doi.org/10.1175/1520-0493(2004)132<1917:aarmmi>2.0.co;2)
- Williams, C. A., & Hanan, N. P. (2011). ENSO and IOD teleconnections for African ecosystems: Evidence of destructive interference between climate oscillations. *Biogeosciences*, 8(1), 27–40. <https://doi.org/10.5194/bg-8-27-2011>
- Wilson, E. A., Gordon, A. L., & Kim, D. (2013). Observations of the Madden-Julian oscillation during Indian ocean dipole events. *Journal of Geophysical Research: Atmospheres*, 118(6), 2588–2599. <https://doi.org/10.1002/jgrd.50241>
- Yadav, R. K., Rupa Kumar, K., & Rajeevan, M. (2009). Increasing influence of ENSO and decreasing influence of AO/NAO in the recent decades over northwest India winter precipitation. *Journal of Geophysical Research*, 114(D12). <https://doi.org/10.1029/2008jd011318>
- Zaitchik, B. F. (2017). Madden-Julian oscillation impacts on tropical African precipitation. *Atmospheric Research*, 184, 88–102. <https://doi.org/10.1016/j.atmosres.2016.10.002>
- Zhang, C. (2005). Madden-Julian oscillation. *Reviews of Geophysics*, 43(2). <https://doi.org/10.1029/2004rg000158>
- Zhang, C., & Dong, M. (2004). Seasonality in the Madden-Julian oscillation. *Journal of Climate*, 17(16), 3169–3180. [https://doi.org/10.1175/1520-0442\(2004\)017<3169:sitmo>2.0.co;2](https://doi.org/10.1175/1520-0442(2004)017<3169:sitmo>2.0.co;2)
- Zhang, C., & Gottschalck, J. (2002). SST anomalies of ENSO and the Madden-Julian oscillation in the equatorial Pacific. *Journal of Climate*, 15(17), 2429–2445. [https://doi.org/10.1175/1520-0442\(2002\)015<2429:saoeat>2.0.co;2](https://doi.org/10.1175/1520-0442(2002)015<2429:saoeat>2.0.co;2)
- Zhou, L., Tian, Y., Myneni, R. B., Ciais, P., Saatchi, S., Liu, Y. Y., et al. (2014). Widespread decline of Congo rainforest greenness in the past decade. *Nature*, 509(7498), 86–90. <https://doi.org/10.1038/nature13265>